Processing and Application of Ceramics 13 [1] (2019) 24–31
https://doi.org/10.2298/PAC1901024H

Fabrication, dielectric and electrical characteristics of 0.94 $(Bi_{0.5}Na_{0.5})TiO_3$-0.06 $BaTiO_3$ ceramics

Sugato Hajra[1,*], Neeha Pradhani[2], Ram Naresh Prasad Choudhary[2], Sushrisangita Sahoo[2]

[1]*Department of Electronics and Instrumentation, Siksha O Anusandhan (Deemed to be University), Bhubaneswar-751030, India*
[2]*Department of Physics, Siksha O Anusandhan (Deemed to be University), Bhubaneswar-751030, India*

Received 12 July 2018; Received in revised form 5 November 2018; Accepted 14 January 2019

Abstract

In the present paper, high temperature synthesis was used to prepare the complex electronic system 0.94 $(Bi_{0.5}Na_{0.5})TiO_3$-0.06 $BaTiO_3$ (BNT-BT-6). The relationship between the structure and electrical properties have been presented. The crystal data (i.e. unit cell dimensions and tetragonal crystal system) was obtained by preliminary structural analysis using room temperature X-ray diffraction spectra. The unequally distributed and densely packed ceramics were observed in the SEM micrograph of the sintered sample. The vibrational modes of BNT-BT-6 system using room temperature Raman and FT-IR spectra were reported. Temperature and frequency dependent dielectric parameters of BNT-BT-6 exhibit the shift in transition temperature, enhancement of dielectric constant and decrease in dissipation factor of BNT on the addition of BT even in a small amount. Analysis of the frequency and temperature dependent electrical modulus and impedance data of the system shows that the material follows non-Debye type of dielectric relaxation process. The overview of grain effect on the capacitive and resistive characteristics of the BNT-BT-6 material was studied experimentally from the Nyquist plots. Analysis of conductivity spectra was used to calculate activation energy and determine the electrical transport mechanism of the material.

Keywords: *$(Bi_{0.5}Na_{0.5})TiO_3$-$BaTiO_3$, solid state reaction, structure, electrical properties, impedance analyses*

I. Introduction

The high dielectric permittivity and low dissipation factor of lead-based ferroelectrics are widely used in electronic industry for coupling-decoupling, bypassing, elimination of unwanted signals, etc. [1]. Unfortunately, such type of ceramic based capacitors has limited function because of their low operating temperature (up to 150 °C). Therefore, there is a great demand to develop electronic systems with ferroelectric properties at elevated operating temperature [2]. Therefore, the development of high temperature dielectrics is really crucial and a big challenge. Moreover, lead oxide (PbO) in lead-based ceramics is highly toxic and dangerous to the environment, and its application is banned in future consumer products by several policies (RoHS/WEEE).

By seeing the environmental concern, investigation of non-toxic lead-free material as an alternative to lead-based ceramics is of great interest. The operational range of thermally stable $BaTiO_3$ (BT) of about 200 °C is a bit restricting. The temperature range for stable dielectric constant has been reported up to 250 °C in Mn/Ca modified ferroelectric $(Bi_{0.5}Na_{0.5})TiO_3$ (BNT) [3,4]. Some ternary systems, namely $BiScO_3$-$BaTiO_3$-$(Bi_{0.5}K_{0.5})TiO_3$ and $BiScO_3$-$(K_{0.5}Na_{0.5})NbO_3$ (KNN), show quite good dielectric stability in a temperature range of 100–300 °C [5,6]. In addition, BNT-BT-$CaZrO_3$ (CZ) shows a variation of permittivity within 15% in the temperature range of 100 to 370 °C, whereas BNT-BT-KNN-CZ shows it in the range of 70 to 470 °C [7].

Although BNT-BT based solid solutions have shown a positive ability towards its uses as a capacitor, a series of scientific problems remain unclear, such as the lack of: i) electrical homogeneity of the material due to chemical complexity, ii) clarity in the dielectric relaxation mechanism at high temperature, etc. The performance and lifespan of ceramic capacitors at high tem-

*Corresponding author: tel: +918908036901,
e-mail: *sugatofl@outlook.com*

peratures can be analysed by the investigation of conduction mechanisms. Impedance spectroscopy is a tool to detect and analyse the above stated conditions. Study of temperature dependence of relaxation mechanisms can identify various electro-active parameters of a sample. In the case of various ferroelectric materials, the imaginary part of impedance as well as modulus gives important information about the spread of the relaxation time. From the literature survey, it is found that the electrical properties along with the similarity of structure are controversial and inconsistent for BNT-BT system. In this context, ceramics with a small amount (6 mol%) of barium titanate added to BNT was fabricated and its microstructure and electrical properties (dielectric, conductivity, impedance, modulus) were investigated.

II. Experimental procedure

2.1. Powder preparation

The polycrystalline sample of a composition 0.94 $(Bi_{0.5}Na_{0.5})TiO_3$-0.06 $BaTiO_3$ (BNT-BT-6) was synthesized by a conventional high-temperature mixed-oxide method using the analytic grade (AR) ingredients of oxides and carbonates: bismuth oxide (99.99%), sodium carbonate (99.5%), barium carbonate (99.99%) purchased from Central drug house and titanium oxide (99.99%; Loba Chemie). The weighed mixture of powder was mixed thoroughly in dry as well as in wet medium using agate mortar. The extra 2 wt.% of Bi_2O_3 was added initially to compensate the loss during the high temperature heating. The resulting mixture was calcined at 850 °C for 4 h using high-purity alumina (Al_2O_3) crucible followed by repeated grinding. After that, the powder was blended along with 5 wt.% of polyvinyl alcohol (PVA). Finally, disc shaped pellets were compacted using a hydraulic press with a pressure range of 4–5 × 10^6 N/m^2. The pellets dimension was 12 mm diameter and thickness of 1.5–1.8 mm. Preheating of the green pellets in an oven was used to remove PVA. Final sintering was at 970 °C for 4 h in a computer programmable furnace in order to densify the samples.

2.2. Characterization techniques

The phase-purity of the sample was checked by using an X-ray diffractometer (Rigaku SmartLab) data collected with CuKα (λ = 0.15406 nm) for a wide Bragg's angle $20° \leq 2\theta \leq 80°$. The gold coated pellet was used to study the texture and morphology of grain distribution at the surface with the help of scanning electron microscope (SEM) (M/s JEOL JSM 840). The spatial distribution of the ions (Bi, Ba, Na, Ti, O) present in the composition was determined by the energy-dispersive X-ray spectroscopy (EDS, Oxford Instruments, UK). The room temperature Raman and Fourier transform infrared spectroscopy (FTIR) data were measured with STR-500 Micro Raman and M/S Shimadzu Co Ltd, Japan, respectively. A sintered pellet was painted with conductive silver paste after being polished with emery paper. The frequency and temperature dependent dielectric properties, conductivity and impedance were measured using a phase sensitive meter (model PSM 1735, N4L). The electrical properties were measured at various frequencies (1–1000 kHz) and temperatures (25–400 °C).

III. Results and discussion

3.1. Structure and morphology

Figure 1 exhibits room temperature X-ray diffraction (XRD) pattern of the sintered BNT-BT-6 ceramics. The location (on 2θ axis) and intensities of all the peaks do not coincide with those of the oxides used for synthesis. Fabrication of nearly pure phase of the desired material was confirmed based on the nature and distribution of peaks [11]. Determination of basic crystal data and structural analysis were carried out using a commercial computer program package "POWD" [12]. The least difference in the experimentally determined and theoretically obtained inter-planar distances (i.e. $\sum d_{obs} - \sum d_{cal}$ = minimum) shows that the prepared material belongs to the tetragonal crystal system. The least-squares lattice parameters are as follows: a = 5.79 Å and c = 15.50 Å which are normalized to a = 5.79 Å, c = 15.50/2 = 7.75 Å, and volume V = 1391.58 Å^3. The impurity peak near 30° corresponds to $BaTiO_3$ (marked with asterisk in Fig. 1) having tetragonal phase (ICDD card No. 04-013-6990). A few smaller intensity un-indexed peaks could relate to the presence of some unknown impurity phase, formed either from the inherent impurities of ingredients or new compound formed during the synthesis [13].

The surface morphology given in the SEM micrograph (Fig. 2) shows a presence of highly packed grains and low porosity. There is an unequal distribution of grains, confirming the presence of a grain growth inhibitor and the compositional fluctuation between A and B sites. The degree of porosity in the sample cannot be measured due to the lack of experimental software.

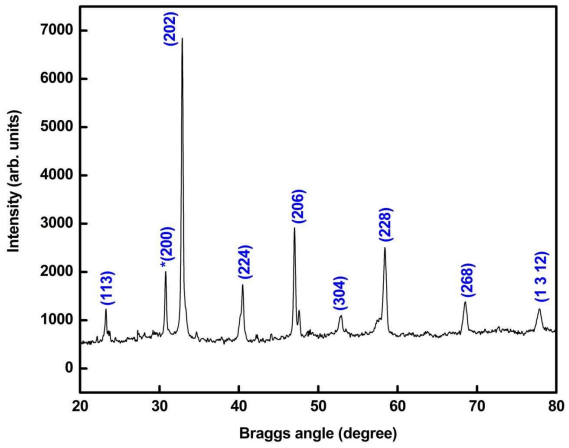

Figure 1. Room temperature XRD spectrum of the sintered BNT-BT-6 sample

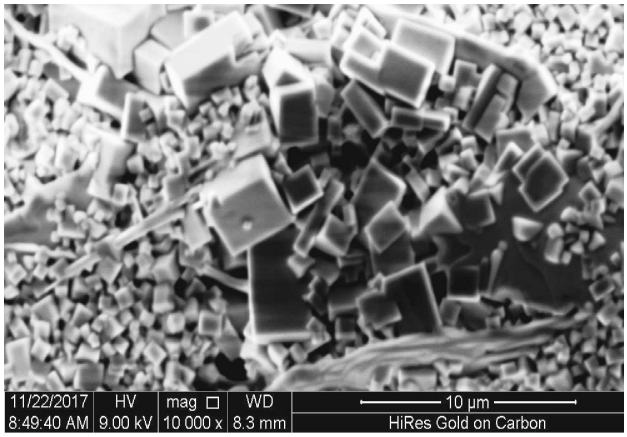

Figure 2. SEM microstructure of BNT-BT-6 sample

Table 1. Composition of sintered BNT-BT-6 sample determined by EDS

Element	Composition	
	[wt.%]	[at.%]
O	32.2	72.7
Na	5.0	7.8
Ti	14.5	10.9
Ba	3.5	0.9
Bi	44.7	7.7

However, the measured density of the sintered BNT-BT-6 ceramics is relatively high, i.e. 95 %TD. The high density packing of grains leads to the structural integrity with enhanced electrical properties of the prepared sample [14]. The sample composition as atomic and weight percentage obtained from EDS is shown in Table 1.

3.2. Raman spectroscopy

The effect of addition of a small amount (6 mol%) of BT on the crystal and molecular structure of BNT was studied by Raman spectroscopy (Fig. 3). By fitting the Raman spectrum with the Gaussian line shapes (using the Origin 8.0 software) six modes could be identified in the frequency range of 130–900 cm^{-1}. The deconvoluted individual components of the total Raman spectrum are located at 141, 274, 522, 576, 783 and 861 cm^{-1}. All these modes are broad; that reflects on the poly-crystalline nature of the sample and disorder due to the random occupancy of cation site A by Na/Bi [15].

The bands situated below 250 cm^{-1} are assigned to Na/Bi–O stretching vibrations (related to AO_4 tetrahedral). It is seen that above 250 cm^{-1}, the bands are mainly associated with Ti–O stretching vibrations (analogous to BO_6 octahedral). In particular, the 274 cm^{-1} mode involves only O–Ti–O bending motion, which is sensitive to the phase transition [16]. At 600–850 cm^{-1} 1 the high-frequency mode corresponds to the TiO_6 oxygen octahedral vibrations [17]. The first Raman active mode at around 141 cm^{-1} is closely associated to distort octahedral [BiO_6] and [NaO_6] clusters. The second Raman active E(TO_2) mode at 274 cm^{-1} occurs due to the presence of octahedral [TiO_6] clusters, which shows the stretching from the bonds. The ionic nature of the lattice causes the short-range electrostatic forces leading to the third Raman-active (LO_2) mode with low intensity. The TO_3 mode around 576 cm^{-1} corresponds to the (–O–Ti–O–) stretching symmetric vibrations of the octahedral TiO_6 clusters [18]. The perovskite structure material basically exhibits this mode. Finally, at 861 cm^{-1}, the LO_3 mode is seen due to the sites within the rhombohedral lattice pre-containing octahedral distorted TiO_6 clusters. Similar results in vibrational spectroscopy have been previously reported earlier [19].

3.3. FTIR analysis

Figure 4 shows the room temperature Fourier transform infrared (FTIR) spectra of the sintered BNT-BT-6 sample over 400–4000 cm^{-1}. The bands in the region of 500–850 cm^{-1} are generally used to find out the stretching vibration of Ti–O bond of the octahedral site in perovskite structure [20]. The bands at 634 and 857 cm^{-1} are assigned to the intrinsic vibrational mode of BNT [21]. The H–O–H bending mode appears at 1708 cm^{-1}. The peak at 1477 cm^{-1} is related to COO vibration. The peak near 946 cm^{-1} corresponds to CO vibrations [22].

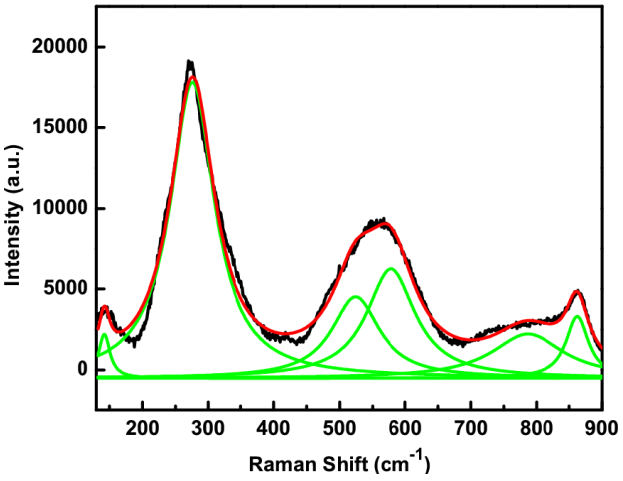

Figure 3. Room temperature deconvoluted Raman spectra of BNT-BT-6

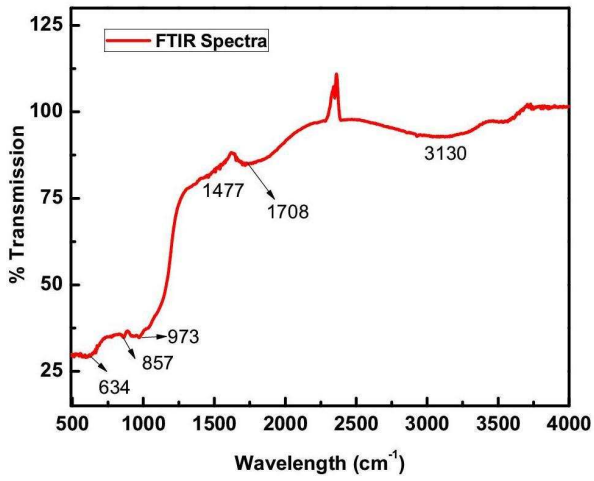

Figure 4. FTIR spectra of BNT-BT-6

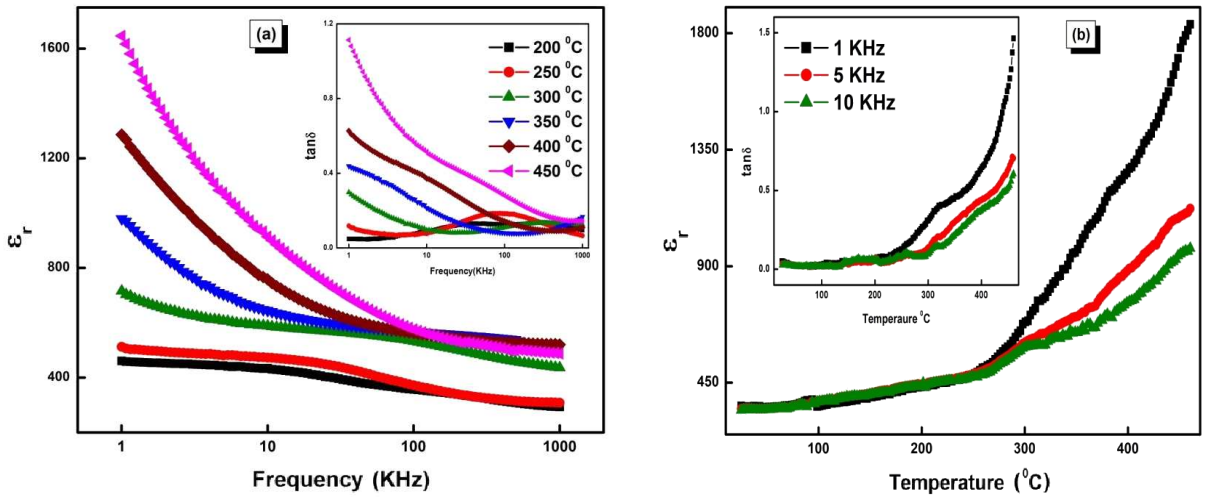

Figure 5. Frequency (a) and temperature (b) dependent dielectric constant and tangent loss of BNT-BT-6

Table 2. Dielectric properties at 500 °C and 1 kHz compared with literature data

Samples	Dielectric constant	Dielectric loss	Ref.
$0.94(Bi_{0.5}Na_{0.5}TiO_3)$–$0.06BaTiO_3$	1838	1.4	Present work
$0.92(Bi_{0.5}Na_{0.5}TiO_3)$–$0.08BaTiO_3$	1180	11.5	[19]
$(Bi_{0.5}Na_{0.5})TiO_3$	1600	0.18	[15]

3.4. Dielectric characteristics

Figure 5a presents the variation of the dielectric constant and tangent loss with frequency and temperatures, and can be seen that both decrease with increasing frequency in a given temperature range range. This variation is typical trend for polar dielectrics or ferroelectrics [23]. At low frequencies, a high dielectric constant (ε_r) indicates highly polar system [24] while increasing the frequency space charge and dipolar polarizations vanish systematically and dielectric constant decreases. The electronic polarization is the fastest and typically persists at frequencies between $\sim 10^{13}$–10^{15} Hz. In contrast, ionic polarization is sluggish and typically occurs at frequencies between $\sim 10^{9}$–10^{13} Hz while dipolar polarization involving movement of molecules happens below 10^{9} Hz. Interface or space charge polarization occurs at frequencies below 10 Hz. Above 100 kHz frequency, the value of dielectric constant becomes frequency independent.

Figure 5b presents the temperature dependence of the dielectric constant and tangent loss. The dielectric constant varies with temperature according to the Curie-Weiss relation [25]:

$$\varepsilon_r = B + \frac{C}{T - T_C} \tag{1}$$

where B and C are temperature independent constants. C and T_C are Curie constant and Curie temperature, respectively. The above relation holds valid for $T > T_C$. The suppression of ferroelectric behaviour may be due to a combination of the elementary dipoles which leads to the dipole alignment (due to an internal field). The reason of depression may be that orientation of the crystal gets distorted from non-centro-symmetric to centro-symmetric. Moreover, there are polar–non-polar symmetry changes and ion diffusion occuring at high temperature [26]. In the low-temperature region, the dielectric loss is small, but at higher temperatures, there is a relative rise in the rate of loss. The rapid change in the dielectric loss at higher temperature may occur due to scattering of temperature dependent charge carriers and the presence of defects/impurity phase in the prepared sample. The measured dielectric properties are noted and compared with other reported data in Table 2.

3.5. Conductivity

Figure 6 presents the effect of temperature on the electrical conductivity (σ_{AC}) of the prepared sample.

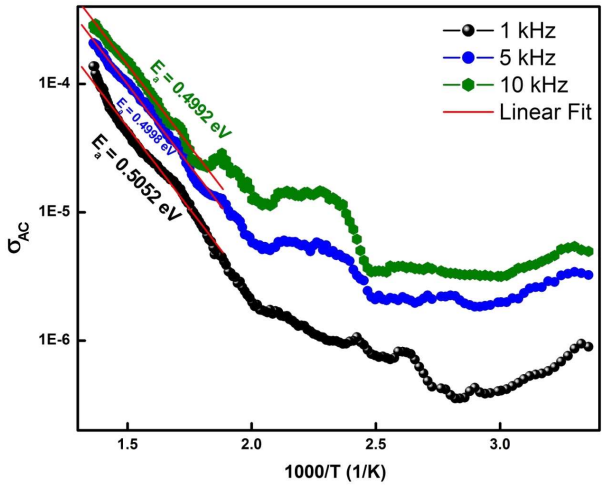

Figure 6. Temperature dependent AC conductivity of BNT-BT-6

Electronic charge carriers, defects and vacancies play a vital role in the conduction mechanism at high temperatures. A frequency independent relation between AC conductivity vs. temperature is calculated as:

$$\sigma = \sigma_0 \exp\left(-\frac{E_a}{k_B T}\right) \tag{2}$$

where σ_0 is a constant, k_B is the Boltzmann constant and E_a is the activation energy for conduction [27]. The activation energies, calculated from temperature dependent AC conductivity plots (in high temperature region), are 0.5052, 0.4998 and 0.4992 eV for the selected frequencies of 1, 5 and 10 kHz, respectively. From these values, it can be suggested that with a rise in frequency the thermal activation energy only slightly decreases. In the studied compound, the electrical conduction is thermally activated process that shows the rise of σ_{AC} with the increase in temperature.

3.6. Impedance

Structure-properties relationship of ionic solid materials is widely analysed with impedance spectroscopy (IS). The various contributions of grains (bulk), grain boundaries and electrode (interface) polarization on resistive parameters can be divided as well as estimated. With variation in the frequency, both resolved components (real and imaginary) of the output signal of complex (*) impedance or modulus can be determined. For this purpose, the components of complex impedance (Z^*) and related parameters (i.e., electrical modulus (M^*), permittivity (ε^*) and admittance (Y^*)) can be calculated from following equations:

$$\tan\delta = \frac{\varepsilon}{\varepsilon'} = -\frac{Z'}{Z''} = \frac{M''}{M'} \tag{3}$$

$$\frac{1}{\varepsilon^*} = M^* = M' + jM'' = j\omega C_0 Z^* \tag{4}$$

$$Z^* = Z' - Z'' = R_s - \frac{j}{\omega C_s} \tag{5}$$

$$\varepsilon^* \varepsilon' - j\varepsilon'' \tag{6}$$

$$Y^* - Y' + Y'' = \frac{1}{R_p} + j\omega C_p \tag{7}$$

Figure 7a presents the frequency and temperature dependence of complex impedance parameters (Z' and Z''). Decrease in Z' is related to the enhancement of electrical conductance of the material with increasing frequency and temperature. The release of space charge is related to the merge of Z' values at high frequencies [28]. The decrease in the value of the real part of impedance (Z') with the rise in temperature at higher frequency depicts the semiconductor nature of the material.

Bode plots are basically preferred over the Nyquist plot as they show the variation of the impedance parameters over a wide frequency range. The variation of Z'' with frequency and temperature is presented in the inset of Fig. 7a. A similar trend is seen for the real component of impedance, the maximum magnitude of Z'' falls smoothly with the rise of frequency and temperature. Finally it merges at higher frequencies, again suggesting the effect of space charge polarization [29]. The temperature dependence of the relaxation phenomenon is observed at low frequencies. The dielectric relaxation in the material occurs due to low-temperature immobile charges as well as high-temperature creation of defects and vacancies [30] etc.

Figure 7b presents the Nyquist plots (i.e., Z' vs. Z'') at selected temperatures. Using such type of plots, the frequency dependence of resistive characteristics of the material is analysed by using a circle or semicircle of the material traced at different temperatures. With an increase of temperature, the plots show the tendency of circular and semi-circular arcs. The centres of the circle or semi-circular arcs formed at elevated temperatures are observed at the Z' or x-axis. The semicircle thus formed is slowly distorted with the centre below the x-axis on a further rise in temperature. The grains and ideal Debye type of dielectric relaxation leads to the formation of the perfect or ideal semicircle. The formation of symmetric semicircle suggests the existence of ideal Debye relaxation, whereas distorted semicircles confirm the presence of non-ideal or non-Debye type of relaxation [31]. As a perfect semicircle due to the grain is not formed, it manifests distribution of multiple relaxation times. Nyquist plot is fitted to an equivalent circuit using "ZSMIP WIN" version 2 commercial software package.

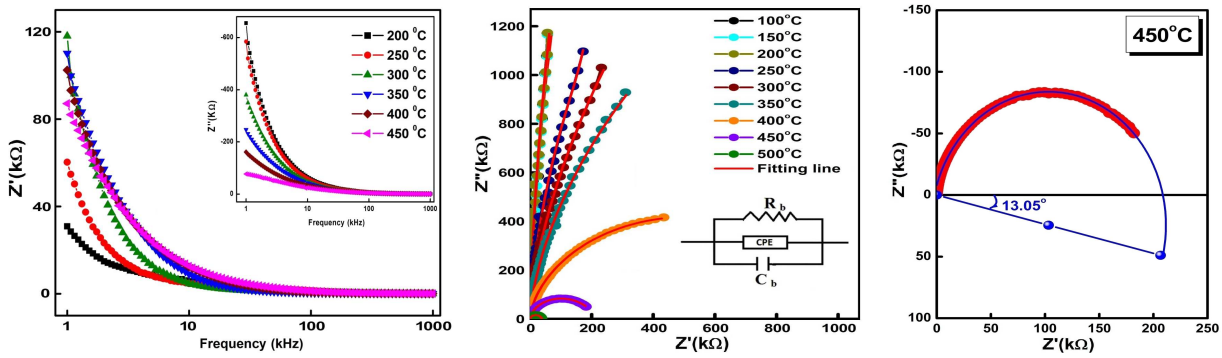

Figure 7. Frequency dependent real and imaginary (inset) part of impedance (a), Nyquist plots at various temperatures from 100 to 500 °C (b) and the depression angle at 450 °C for BNT-BT-6 sample

Table 3. The values of grain resistance (R_g) and grain capacitance (C_g) at various temperatures calculated using RQC

T [°C]	R_g [MΩ]	C_g [pF]
100	75.41	124.5
150	29.82	28.77
200	36.29	0.012
250	10.29	116.2
300	12.79	122.3
350	5.665	116.8
400	1.116	114.8
450	0.219	111.5
500	0.0394	104.0

A suitable electrical circuit (RQC) was used for fitting of the experimental complex impedance response (inset in Fig. 7b). The values of grain capacitance and resistance of the sample at various temperatures are given in Table 3. It is observed that with an increase in temperature the grain/bulk resistance decreases, so the prepared sample exhibits negative temperature coefficient of resistance (NTCR) behaviour. The non-Debye relaxation mechanism was also revealed from Fig. 7c. The depression angle of 13.05° at 450 °C suggests that the centre is located below the real Z-axis.

3.7. Electrical modulus

The electrical modulus analysis gives much vital information on the dielectric relaxation process of non-conducting materials, polycrystalline ceramics and vitreous ionic conductors where impedance technique does not work well [32]. Figure 8a shows the systematic change in the real part of modulus with variation in electric field (frequency) at different temperatures. At high frequency, dielectric dispersion peak due to the real part of modulus moves towards its asymptotic value. The dielectric dispersion shifts to the higher side of the frequency range. At low temperatures, systematic change in the above dispersion is caused by mobility of the charge carriers at short range. This situation occurs because of the absence of the recovery force for charge carrier mobility on the increase of the frequency. Figure 8b shows the effect of frequency on the imaginary part of modulus at various temperatures. The maximum value of the imaginary component (M''_{max}) is shifted towards the higher side of frequency range with the temperature rising. A better correlation between mobility of charge carriers and the peak value of M'' can be seen [33]. It is observed that at 200 °C basically there are presence of two humps which may depict the major effect of grain and minor grain boundary effect. The grain effect is dominant over the grain boundary effect in the low frequency region. As it is not clearly visible in the frequency dependent imaginary part of impedance, the variation of M'' over frequency is plotted to see the minor effect of grain boundary if present. There is a non-symmetric broadening of M'' peak. It depicts the distribution of dielectric relaxation with multiple time constant. The range of peak frequencies suggests transition of motion of charge carrier from short to long range [34].

IV. Conclusions

The paper is mainly focused on fabrication of lead-free (BNT-BT-6) perovskite ceramics by a cost-effective processing route at high temperature. Fabrication of nearly pure tetragonal perovskite phase of the desired material was confirmed based on the nature and distribution of peaks. SEM microstructure shows high density grain growth. The low dielectric loss and the compacted density of sample manifest a low loss material. The complex impedance and modulus spectroscopy combined with conductivity analysis showed the prepared material to be of non-Debye type with NTCR behaviour. The activation energy for conductivity of the prepared sample was estimated. Thus, the above results show that prepared composition could be feasible alternative for eco-friendly lead-free ceramics and may serve as a base for device engineering.

Acknowledgement: The authors like to express their sincere gratitude to Mr. Manojit De and Dr. HS Tiwari

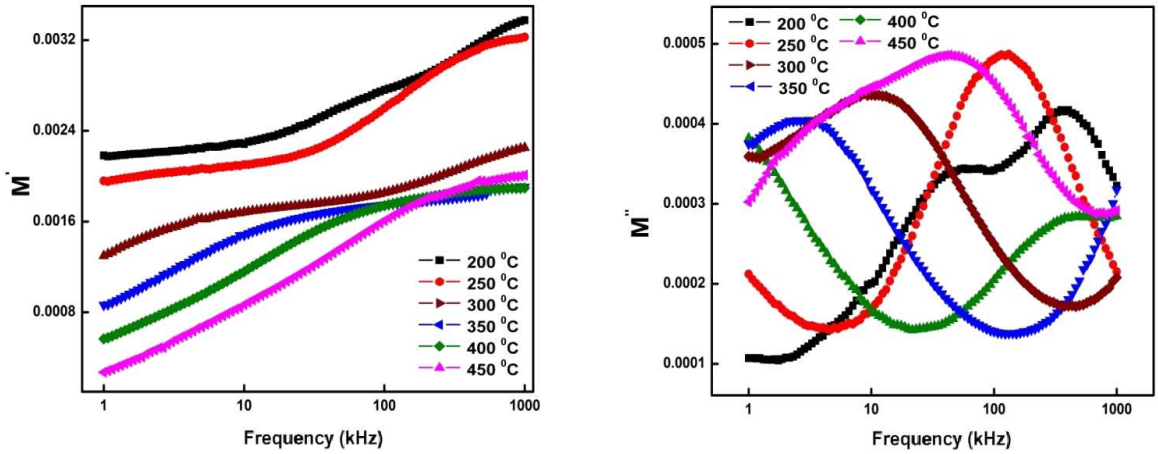

Figure 8. Frequency dependent real (a) and imaginary (b) part of modulus for BNT-BT-6

of Guru Ghasidas Central University, Bilaspur, India for carrying out the Raman and FT-IR spectra of the sample in their laboratory. Dr. Kalyani Mohanta IIT BHU is thankful for the SEM experiment.

References

1. A. Nishino, "Capacitors: operating principles, current market and technical trends", *J. Power Sources*, **60** (1996) 137–147.
2. R.W. Johnson, J.L. Evans, P. Jacobsen, J.R. Thompson, M. Christopher, "The changing automotive environment: high-temperature electronics", *IEEE Trans. Electron. Package Manuf.*, **27** (2004) 164–176.
3. Y. Yuan, E.Z. Li, B. Li, B. Tang, X.H. Zhou, "Effects of Ca and Mn additions on the microstructure and dielectric properties of $(Bi_{0.5}Na_{0.5})TiO_3$ ceramics", *J. Electron. Mater.*, **40** (2011) 2234–2239.
4. R. Ranjan, V. Kothai, R. Garg, A. Agrawal, A. Senyshyn, H. Boysen, "Degenerate rhombohedral and orthorhombic states in Ca-substituted $Na_{0.5}Bi_{0.5}TiO_3$", *Appl. Phys. Lett.*, **95** (2009) 042904.
5. M. Izumia, K. Yamamoto, M. Suzuki, Y. Noguchi, M. Miyayama, "Large electric-field-induced strain in $(Bi_{0.5}Na_{0.5})TiO_3$–$(Bi_{0.5}K_{0.5})TiO_3$ solid solution single crystals", *Appl. Phys. Lett.*, **93** (2008) 242903.
6. X. Sun, J. Chen, R. Yu, C. Sun, G. Liu, X. Xing, L. Qiao, "$BiScO_3$ doped $(Na_{0.5}K_{0.5})NbO_3$ lead-free piezoelectric ceramics", *J. Am. Ceram. Soc.*, **92** (2009) 130–132.
7. M. Chandrasekhar, P. Kumar, "Synthesis and characterizations of BNT-BT-KNN ceramics for energy storage applications", *Phase Transitions*, **89** (2016) 944–957.
8. T. Takenaka, K. Maruyama, K. Sakata, "$(Bi_{1/2}Na_{1/2})TiO_3$-$BaTiO_3$ system for lead-free piezoelectric ceramics", *Jpn. J. Appl. Phys.*, **30** (1991) 2236–2239.
9. A.B. Kounga, S.-T. Zhang, W. Jo, T. Granzow, J. Rodel, "Morphotropic phase boundary in $(1-x)Bi_{0.5}Na_{0.5}TiO_3$–$xK_{0.5}Na_{0.5}NbO_3$ lead-free piezoceramics", *Appl Phys Lett.*, **92** (2008) 222902.
10. A.S. Bhalla, R. Guo, R. Roy, "The perovskite structure – A review of its role in ceramic science and technology", *Mater. Res. Innovations*, **4** (2000) 23–26.
11. H.P. Klug, L.E. Alexander, *X-ray Diffraction Procedures: For Polycrystalline and Amorphous Materials*, Wiley, Chester, England, 1974.
12. E.W. Powd, *An Interactive Powder Diffraction Data Interpretation and Indexing Program, Version 2.1*, School of Physical Science, Flinders University of South Australia, Bedford Park, SA5042, Australia
13. P.P. Rao, S.K. Ghosh, P. Koshy, "Dielectric and ferroelectric properties of $Ba_3M_3Ti_5Nb_5O_{30}$ (M = Sm or Y) ceramics", *J. Mater. Sci.: Mater. Electron.*, **12** (2001) 729–732.
14. Z.P. Yang, B. Liu, L.L. Wei, Y.T. Hou, "Structure and electrical properties of $(1-x)Bi_{0.5}Na_{0.5}TiO_3$–$xBi_{0.5}K_{0.5}TiO_3$ ceramics near morphotropic phase boundary", *Mater. Res. Bull.*, **43** (2008) 81–89.
15. B.K. Barick, K.K. Mishra, A.K. Arora, R.N.P. Choudhary, D.K. Pradhan, "Impedance and Raman spectroscopic studies of $(Na_{0.5}Bi_{0.5})TiO_3$", *J. Phys. D: Appl. Phys.*, **44** (2011) 355402.
16. J. Kreisel, A.M. Glazer, P. Bouvier, G. Lucazeau, "High-pressure Raman study of a relaxor ferroelectric: The $(Na_{0.5}Bi_{0.5})TiO_3$ perovskite", *Phys. Rev. B*, **63** (2001) 174106.
17. J. Kreisel, A.M. Glazer, G. Jones , P.A. Thomas , L. Abello, G. Lucazeau, "An X-ray diffraction and Raman spectroscopy investigation of A-site substituted perovskite compounds: the $(Na_{1-x}K_x)_{0.5}Bi_{0.5}TiO_3$ ($0 \le x \le 1$) solid solution", *J. Phys.: Condens. Matter*, **12** (2000) 3267–3280.
18. P.S. Dobal, A. Dixit, R.S. Katiyar, Z. Yu, R. Guo, A.S. Bhalla, "Micro-Raman scattering and dielectric investigations of phase transition behavior in the $BaTiO_3$-$BaZrO_3$ system", *J. Appl. Phys.*, **89** (2001) 8085–8091
19. S. Sahoo, S. Hajra, M. De, R.N.P. Choudhary, "Resistive, capacitive and conducting properties of $Bi_{0.5}Na_{0.5}TiO_3$–$BaTiO_3$ solid solution", *Ceram. Int.*, **44** (2017) 4719–4726.
20. K. Parmar, N.S. Negi, "Influence of Na/Bi excess on structural, dielectric and multiferroic properties of lead free $(Na_{0.5}Bi_{0.5})_{0.99}La_{0.01}Ti_{0.988}Fe_{0.012}O_3$ ceramic", *J. Alloys Compd.*, **618** (2015) 781–787.
21. A. Paul Blessington Selvadurai, V. Pazhnivelu, B.K. Vasanth, C. Jagadeeshwaran, R. Murugaraj, "Investigation of structural and optical spectroscopy of 5% Pr doped $(Bi_{0.5}Na_{0.5})TiO_3$ ferroelectric ceramics: site depended study", *J. Mater. Sci.: Mater. Electron.*, **26** (2015) 7655–7665.
22. R. Urlaub, U. Posset, R. Thull, "FT-IR spectroscopic investigations on sol-gel-derived coatings from acid-modified titanium alkoxides", *J. Non-Cryst. Solids*, **265** (2000) 276–284.
23. R.N.P. Choudhary, K. Perez, P. Bhattacharya, R.S. Katiyar, "Structural and electrical properties of $BiFeO_3$-$Pb(ZrTi)O_3$ composites", *Appl. Phys. A*, **86** (2007) 131-138.
24. S. Pattanayak, B.N. Parida, P.R. Das, R.N.P. Choudhary, "Impedance spectroscopy of Gd-doped $BiFeO_3$ multiferroics", *Appl. Phys. A*, **112** (2013) 387–395.
25. N. Bassiri-Gharb, *Dielectric and Piezoelectric Nonlinearity in Oriented $Pb(Yb_{1/2}Nb_{1/2})O_3$-$PbTiO_3$ Thin Films*, Doctoral Thesis Dissertation, The Pennsylvania State University, 2005.
26. M. Szafranski, M. Jarek, "Origin of spontaneous polarization and reconstructive phase transition in guanidinium iodide", *Cryst. Eng. Commun.*, **15** (2013) 4617–4623.
27. A.K. Jonscher, "The 'universal' dielectric response", *Nature*, **267** (1977) 673–679.
28. S. Nath, S.K. Barick, S. Hajra, R.N.P. Choudhary, "Studies of structural, impedance spectroscopy and magnetoelectric properties of $(SmLi)_{1/2}(Fe_{2/3}Mo_{1/3})O_3$ electroceramics", *J. Mater. Sci.: Mater. Electron.*, **29** (2018) 12251–12257.
29. B. Behera, P. Nayak, R.N.P. Choudhary, "Structural and impedance properties of $KBa_2V_5O_{15}$ ceramics", *Mater. Res. Bull.*, **43** (2008) 401–410.
30. C.K. Suman, K. Prasad, R.N.P. Choudhary, "Complex impedance studies on tungsten-bronze electroceramic: $Pb_2Bi_3LaTi_5O_{18}$", *J. Mater. Sci.*, **41** (2006) 369–375.
31. A.R. West, D.C. Sinclair, N. Hirose, "Characterization of electrical materials, especially ferroelectrics, by impedance spectroscopy", *J. Electroceram.*, **1** (1997) 65–71.
32. P. Sharma, S. Hajra, S. Sahoo, P.K. Rout, R.N.P. Choudhary, "Structural and electrical of gallium modified PZT ceramics", *Process. Appl. Ceram.*, **11** (2017) 171–176.
33. F. Borsa, D.R. Torgeson, S.W. Martin, H.K. Patel, "Relax-

ation and fluctuations in glassy fast-ion conductors: Wide-frequency-range NMR and conductivity measurements", *Phys. Rev. B*, **46** (1992) 795–800.

34. J.R. Macdonald, "Note on the parameterization of the constant-phase admittance element", *Solid State Ionics*, **13** (1984) 147–149.